AIAA JOURNAL
Vol. 46, No. 6, June 2008

Investigation by Particle Image Velocimetry Measurements of Oblique Shock Reflection with Separation

P. Dupont* and S. Piponniau†
Institut Universitaire des Systèmes Thermiques Industriels, Université de Provence and Unité Mixte de Recherche Centre National de la Recherche Scientifique N°6595, 13003 Marseille Cedex 13, France
A. Sidorenko‡
Institute of Theoretical and Applied Mechanics, Siberian Branch, Russian Academy of Sciences, 630090, Novosibirsk, Russia
and
J. F. Debiève§
Institut Universitaire des Systèmes Thermiques Industriels, Université de Provence and Unité Mixte de Recherche Centre National de la Recherche Scientifique N°6595, 13003 Marseille Cedex 13, France

DOI: 10.2514/1.30154

The organization and length scales of turbulent structures and unsteadiness generated in a shock-wave-induced separation at Mach number of 2.3 are investigated experimentally using particle image velocimetry. Processing of the velocity fields displays and demonstrates the existence of structures in the mixing layer developed in the separation bubble. Moreover, we show in evidence a link between the reflected shock excursions and the size of the separated flow. This overview of the spatial organization of the interaction provides a more comprehensive picture of the flow.

Nomenclature

C_f	=	friction coefficient
L	=	length of the interaction
M	=	Mach number
Re_θ	=	Reynolds number based on the momentum thickness
S_L	=	Strouhal number
T_t	=	stagnation temperature
U_0	=	upstream external velocity
U^+	=	V/u_τ
u_τ	=	friction velocity
V	=	Van Driest transformed velocity
X^*	=	$(x - X_0)/L$
X_0	=	mean position of the reflected shock
x	=	longitudinal coordinate
Y^*	=	y/δ_0
y	=	normal to the wall coordinate
y^+	=	yu_τ/ν
δ_0	=	upstream boundary-layer thickness
θ	=	incidence angle of the shock generator
ν	=	kinematic viscosity

Presented as Paper 119 at the 45th AIAA Aerospace Sciences Meeting and Exhibit, Reno, NV, 8–11 January 2007; received 31 January 2007; accepted for publication 5 December 2007.

*Chargé de Recherche, Groupe Supersonique, 12 Aue du Gal Leclerc. Member AIAA
†Ph.D. Student Centre National d'Etudes Spatiales, Groupe Supersonique, 12 Aue du Gal Leclerc.
‡Senior Researcher, Hypersonic Flow Laboratory, Institutskaya, 4/1. Member AIAA.
§Chargé de Recherche, Groupe Supersonique, 12 Aue du Gal Leclerc.

I. Introduction

In many aeronautical applications, critical situations can be produced by the unsteadiness occurring when the boundary layer separates, for example, in backward or forward steps, or in cavity problems. In high-velocity flows, separation can be associated with, or even created by, shock waves that constitute new sources of unsteadiness, generally at frequencies much lower than the energetic eddies of the incoming turbulent boundary layer. This is the case, for example, with wall bumps in transonic flows or shock wave boundary-layer interactions in shock reflection configurations and in ramp flows. This type of flow has been partly documented in the past [1,2] and in more recent reviews [3,4]. Nevertheless, most of the published results consider mean velocity fields (obtained by traditional methods such as pitot probes, laser Doppler anemometry) or unsteady wall pressure measurements. More recently, new optical measurement methods, such as particle image velocimetry or planar laser scattering [5–7], have provided better knowledge of the unsteady aspects of such flows. Nevertheless, some important questions still remain unresolved: in particular, the origin of the low frequency of the shock motion and its coupling with the upstream or downstream flows are not clearly understood. Some authors propose to relate these low-frequency movements to instantaneous behavior of the upstream turbulent boundary layer [7–9]. They found that some low-frequency events of the upstream boundary layer, associated with longitudinal streaks developing near the wall, could be related to certain movements of the detached shock in the case of a Mach 5 ramp flow. Other works have put in evidence strong statistical links between these low-frequency shock oscillations and the dynamics of the detached region which develops downstream [6,10–12]. Finally, recent work based on global linear stability of an interaction between an incident shock wave and a laminar boundary layer [13] has shown that intrinsic three-dimensional global modes at very low frequency can develop inside the interaction, when the shock intensity reaches a critical level, with a strong coupling between the reflected shock and the detached region.

Moreover, some recent works have shown that these flows can now be significantly described by numerical simulations [14–16]. For example, large-eddy simulations (LES) are now able to produce accurate descriptions of the global organization of the incident shock

wave/boundary-layer interaction [14]. However, due to current computer limitations, it is still difficult to simultaneously resolve the low-frequency unsteadiness of the flow together with large computing domains to simulate the flow's three-dimensional properties. Thus, further work is needed to improve numerical methods and understanding of the possible couplings between the different sources of unsteadiness.

In this paper, we will present experimental results obtained at Institut Universitaire des Systèmes Thermiques Industriels (IUSTI). An interaction between an oblique shock wave and a turbulent boundary layer at a Mach number of 2.3 is considered. The shock intensity is strong enough to make the boundary layer separate: the main characteristics of this type of interaction have been described in several previous papers [1,14,17]. Here, we will focus on the unsteady aspects of the interaction. We present results performed with particle image velocimetry (PIV). This method is now well developed and can be applied even in supersonic conditions with reverse flows, with a spatial resolution on the order of 1 mm^2 or even smaller. This is really large enough to describe accurately the energetic scales of these flows. Illustration of the accuracy of PIV measurements will be given in the upstream turbulent boundary layer and compared with laser Doppler anemometry (LDA) results. We will focus on the organization of the recirculating zone and the large scales that develop within, and cover a wide range of frequencies and wave numbers. The results deduced from PIV measurements will be compared with previous results deduced from unsteady wall pressure, LDA, and hot-wire measurements.

II. Experimental Setup

The experiment is carried out in the Mach 2.3 hypoturbulent supersonic wind tunnel at IUSTI. This is a continuous facility with a closed-loop circuit. The test section is 120 mm high and 170 mm wide. The nominal conditions of the interaction are as follows. The incoming boundary layer is turbulent, fully developed, and has a thickness $\delta_0(99\%U_0)$ of 11 mm, an incompressible momentum thickness of 1.28 mm, and a Reynolds number based on the momentum thickness Re_θ of 6.9×10^3. The friction coefficient C_f is 2×10^{-3} and the total temperature is 300 K.

A shock generator made of a sharp-edged plate is fixed on the ceiling of the wind tunnel. It is placed in the freestream and its leading edge is located in the external flow. It spans the entire width of the test section and generates an oblique shock wave impinging on the floor boundary layer. Its angle with respect to the external flow θ can be set continuously up to 10 deg.

The global organization of the incident shock wave boundary-layer interaction obtained by spark schlieren visualization is presented in Fig. 1. The flow deviation due to the incident shock is 8 deg and the pressure gradient is strong enough for the layer to separate. In this case, the incident shock is reflected near the Mach line as an expansion wave, whereas the leading reflected shock originates upstream of the recirculating zone as described in Delery and Marvin [1]. The compression waves located in the relaxation zone, needed to turn back the flow parallel to the wall after its passage through the expansion fan, are barely visible on this visualization.

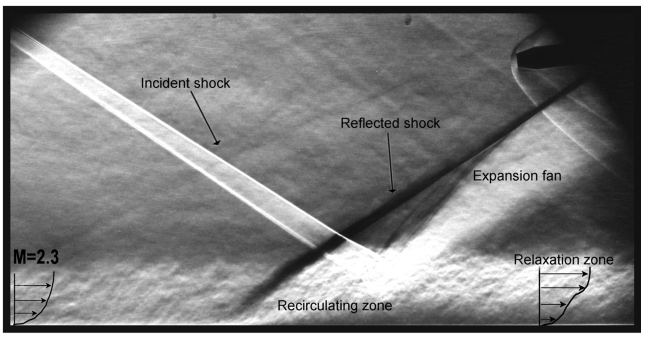

Fig. 1 Spark schlieren visualization of the interaction, flow deviation of 8 deg.

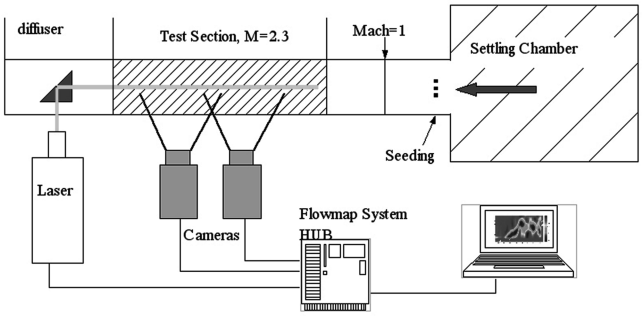

Fig. 2 Sketch of the PIV measurement arrangement.

The origin of the longitudinal coordinate x is chosen at the mean position of the reflected shock at the wall X_0. The length of interaction L is defined as the distance between X_0 and the extrapolation to the wall of the incident shock; it is used to normalize the longitudinal coordinate x. The dimensionless coordinate is therefore $X^* = (x - X_0)/L$, and the interaction extends from $X^* = 0$ to 1.

The PIV investigation is made using a Dantec Dynamics system. The light sheets are generated by a double pulse ND:YAG laser New Wave Solo II, which delivers 30 mJ per pulse, separated in time by 1 μs. The measurements are made in vertical planes, along the longitudinal axis of the wind tunnel. Because of the presence of the shock generator on the ceiling, some optical arrangements are necessary to illuminate the test section: a prism is placed in the diffuser to let the laser sheet propagate back to the measurement area (Fig. 2).

Ten thousand sets of digital images are captured using Flowsense cameras (1600×1200). In the case of 9.5 deg, where the interaction increases significantly, two cameras are lined up next to each other in the longitudinal direction, as shown in Fig. 2, to provide a wide field of view. The two pictures recorded by each camera overlap by approximately 10%. A panoramic grid of calibration is recorded, and the spatial intercorrelation function between pictures gives the spatial correspondence between each field. A global panoramic picture is then created, covering an area of approximately 180×20 mm^2 ($\approx 16\delta_0 \times 2\delta_0$). Nikon Macro Nikkor 60 mm f/2.8 lenses were used on both cameras.

The acquisitions are made via the Dantec Flowmap System Hub. A peculiarity of this system is an internal storage, thus allowing long acquisition samples at a high rate (15 Hz using the two cameras in half-frame mode). Ten thousand images are acquired with two cameras for a shock generator angle of 9.5 deg, corresponding to about 10 min of acquisition. Only one camera is used for the case using an angle of 8 deg.

Incense smoke is used as seeding particles. After decantation of smoke, the particles are injected from the wall, upstream of the sonic section, through 3 holes spaced 10 mm apart and placed symmetrically with respect to the wind-tunnel axis. As the wind-tunnel stagnation pressure is less than atmospheric, the particles are naturally sucked into the flow. The burnt incense particles are an oil-based substance with a density of 800 kg/m^3. Based on the ability of the particles to follow the step of velocity across the incident shock in the external flow, a typical particle size of 1 μm and an equivalent time response in the Lagrangian frame of reference of about 20 μs have been estimated [18].

The images are processed with the Dantec software Flowmanager 4.6. The calibration factor of the pictures is 17 pixels/mm. The intercorrelation is carried out recursively from a cell of size 128×64 to a final cell size of 32 pixels horizontally by 16 pixels vertically, with a Gaussian weighting window applied to the interrogation cell. Therefore, the final effective cell size is 16×8 pixels; this leads to a PIV resolution of 1×0.5 mm^2. Therefore, the accuracy of the velocity measurements, with a subpixel refinement of 0.1 pixel, can be estimated on the order of 6 ms^{-1}. This is believed adequate for taking into account the high velocity gradients perpendicular to the wall inside the incoming boundary layer, as it will be shown in the next section. In the

upstream region of the interaction, a validation rate over 90% is obtained down to $y/\delta_0 = 0.07$ (or $y = 0.8$ mm). This indicates a seeding particle concentration adapted to the size of the cell of analyses. An overlap of 75% between cells provides a field of 390×80 vectors.

To have reference measurements to validate the PIV results, LDA measurements have been carried out inside the upstream boundary layer with a two component system operated in forward scatter mode. The probe volume is an ellipsoid of $(0.2 \times 0.2 \times 1)$ mm^3, taking into account the off-axis setting of the receptive head. The same seeding as in the PIV measurements is used. Measurements of first- and second-order statistical moments of longitudinal and transverse velocity fluctuations obtained with both methods are compared in Figs. 3 and 4. The mean velocity and the standard deviation of the velocity are normalized by the upstream external mean velocity of the flow U_0. Results are found to be in very good agreement, which suggests that the space resolution of our PIV measurements is correctly adapted to the regions of high velocity gradient.

The mean velocity fields obtained by PIV provides a global description of the mean spatial organization of the flow. For example, the spatial map of longitudinal rms fluctuations for the $\theta = 9.5$ deg case are reported in Fig. 5. A strong increase of the boundary-layer thickness is observed together with the development of very high levels of turbulence downstream of the reflected shock.

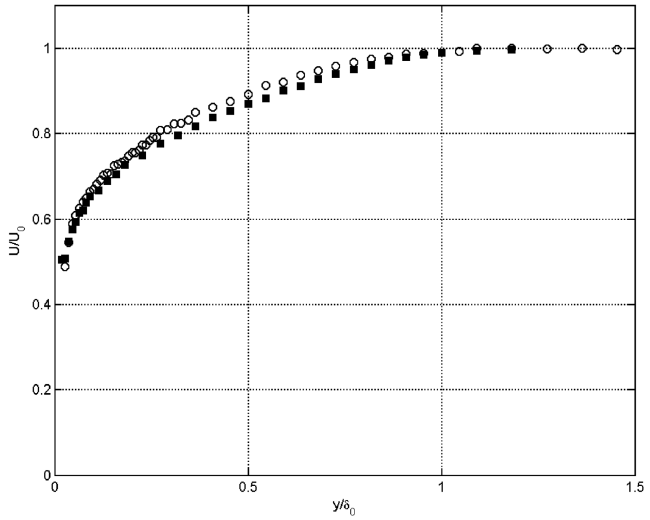

Fig. 3 Comparison of the mean longitudinal velocity deduced from LDA (open symbols) and PIV (closed symbols) measurements in the upstream turbulent boundary layer.

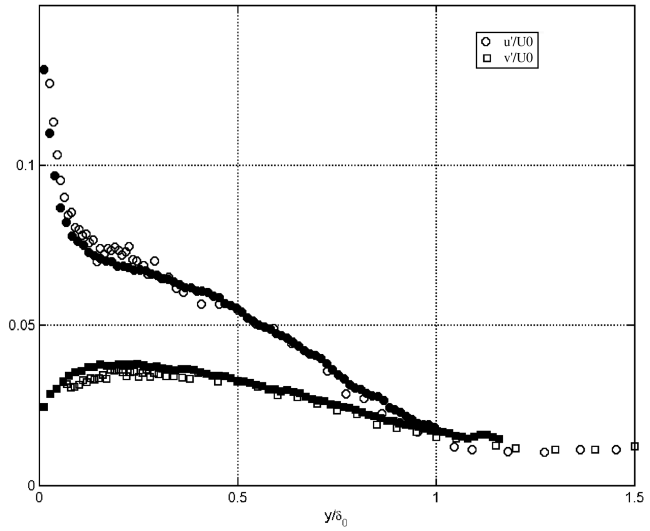

Fig. 4 Comparison of the turbulence intensity deduced from LDA (open symbols) and PIV (closed symbols) measurements in the upstream boundary layer.

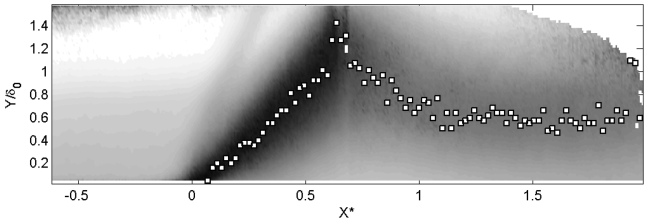

Fig. 5 Map of the rms longitudinal velocity (u'/U_0) for $\theta = 9.5$ deg. Dots correspond to the local maximum of the rms profile.

This region of high level of turbulence starts near the wall, just downstream of the foot of the reflected shock, then moves up in the layer (up to $y/\delta_0 \approx 1$), and continues far downstream of the end of the interaction. The unsteady reflected shock cannot be clearly identified from these maps: the artificial turbulent intensity due to its oscillations is too small compared with the turbulence generated inside the interaction. On the other hand, if normal rms velocity fluctuations are considered for $y/\delta_0 > 0.6$, the turbulence intensity just upstream and downstream of the region of the shock movements are smaller than the artificial turbulence intensity of the vertical fluctuations velocity due to the reflected shock oscillations (see Fig. 6).

Therefore, an evaluation of the mean position of the reflected shock is derived from the transverse velocity fluctuation maps. The shock is supposed to generate a constant step of a given quantity q and to move randomly around its mean position $X_0(y)$ over a space length $L_{\text{ex}}(y)$. The quantity q can be any quantity related to the shock effect: pressure, a component of velocity, momentum, etc. Its upstream value is noted q_0. For the sake of simplicity, the level of turbulence upstream and downstream of the shock are neglected. Then, the first- and second-order moments of the quantity q can be written as functions of the intermittency factor γ, related to the presence of the shock at a given position, and the step of the quantity across the shock Δq (see [11]for details):

$$\frac{\bar{q} - q_0}{\Delta q} = \gamma \quad \text{and} \quad \frac{\sigma_q}{\Delta q} = \sqrt{\gamma(1-\gamma)}$$

Therefore, the median position of the shock ($\gamma = 1/2$) corresponds to the maximum of σ_q/Δq. The extent of the region of oscillation L_{ex} is related to the extent of the bump of $\sigma q/\Delta$q. It has been arbitrarily defined as the point where this quantity is reduced by a factor $1/e$.

This procedure has been applied for different shock generator angles. The associated length of interaction is obtained by extrapolation to the wall of the position of the shock. Results are summarized in Fig. 7. They are compared with previous determinations in the same flow configuration by other methods: 1) schlieren determination with adiabatic or heated wall [19,20], and 2) wall pressure fluctuations measurements [6], where the same procedure as for rms normal velocity has been used.

The length of shock excursion has also been estimated from hot-wire measurements for $y = 1.5\delta_0$. The value deduced from the hot-wire data and the PIV measurements are, respectively, 10.5 and 12 mm.

In spite of the blurring due to the particles inertia in our experimental conditions, we obtain a determination of the shock

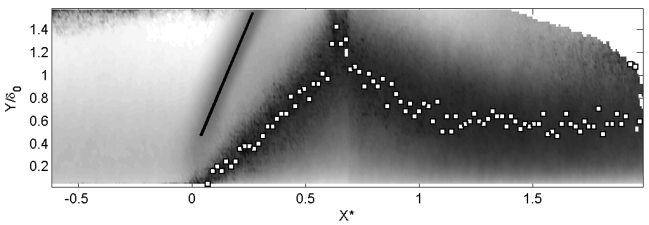

Fig. 6 Map of the rms transverse velocity (v'/U_0) for $\theta = 9.5$ deg; dots correspond to the local maximum of the rms profile; solid line corresponds to the localization of the mean position of the unsteady reflected shock.

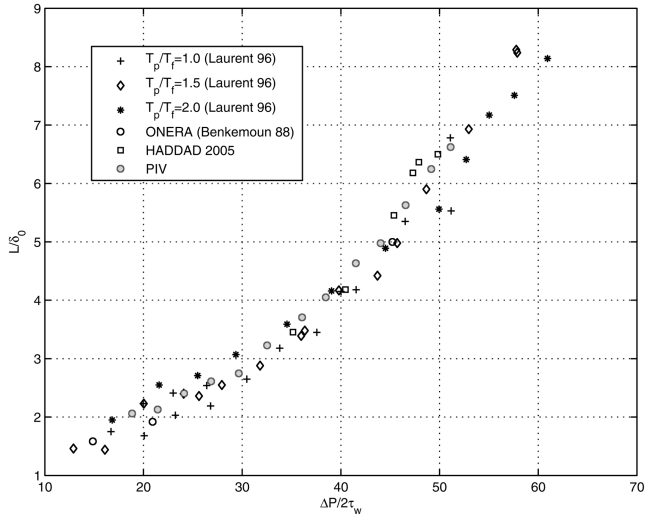

Fig. 7 Determination of length of interaction by PIV measurements, schlieren visualization, and wall pressure measurements. Separated interactions for $\Delta p/2\tau_w > 30$, where ΔP is the pressure step across the incident shock.

position and domain of shock oscillations in good agreement with the schlieren visualizations, the wall pressure, and the hot-wire measurements.

III. Large Scale Eduction Inside the Interaction

As mentioned in the previous section, the development of a region with a high level of turbulence, and with maximum of turbulence intensity far from the wall, can be observed downstream of the reflected shock. This region of maximum turbulence detached from the wall is still present in the relaxation zone ($X^* > 1$), where the maximum is reached at $y/\delta_0 \approx 0.5$.

The typical mean longitudinal velocity profile in the middle of the interaction is presented Fig. 8. It is very similar to velocity profiles observed in subsonic separated flows [21] and can be compared with mixing layer profiles. Such cases, with reverse flow and inflexional velocity profiles, are known to develop large convective eddies, due to the Kelvin–Helmholtz instability.

The instantaneous velocity fields obtained in the present work confirm the development of large eddies in the region of separated flow. A characteristic example is presented in Fig. 9. On this figure, a constant convection velocity is removed to enhance the large convective scales which are developing in the detached zone. To estimate this convection velocity, we can remark that, in the frame of

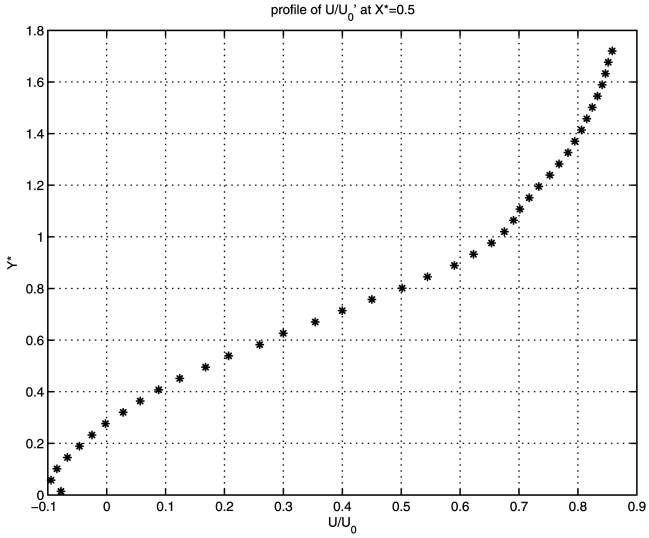

Fig. 8 Mean longitudinal velocity in the recirculating zone, $X^* = 0.5$.

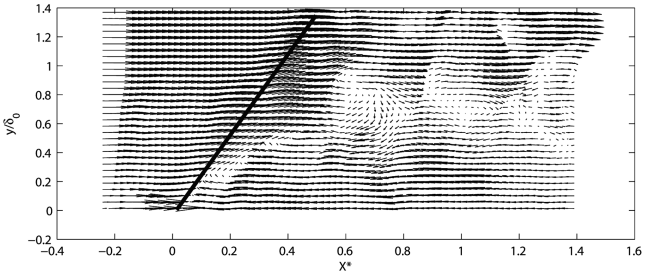

Fig. 9 Instantaneous velocity field inside the interaction. The solid line corresponds to the mean position of the reflected shock.

reference of a convected vortex, the average modulus of the velocity on a domain containing the eddy is smaller than for any other frame of reference. This property has been used to estimate the convection velocity of several eddies: values ranging between 160 and 230 ms^{-1} have been obtained. It has been controlled that such results do not depend significantly on the convection velocity for this range of values, and a median value of 200 ms^{-1} has been retained.

The initial part of the interaction ($X^* < 0.5$) clearly develops vortical structures with successive roll up. The scales are on the order of 0.2 initial boundary-layer thickness. In the second part of the interaction ($X^* > 0.5$), larger eddies are created and shed downstream with characteristic wavelength, on the order of $0.4L$ for the instantaneous field presented in Fig. 9.

To describe the dynamics of this mixing-layer-like flow, an attempt has been made to localize and analyze these structures from the PIV data set. The problem is that the detection of vortices on instantaneous fields with classical criteria, based mainly on the decomposition of the local velocity gradient or the vorticity, can lead to confusing results due to the small scale turbulence on the instantaneous velocity field and to the presence of unvalidated or false vectors. To localize the center of the large scale vortices in our set of data, a nonlocal criterion Γ_1 proposed by Graftieaux et al. [22] is used. It is based on the topology of the velocity field, and is defined in the following way:

Let P be a point of the vector field, S a two-dimensional area surrounding P, and M a point of this area. The vorticity detector Γ_1 is defined as

$$\Gamma_1(P) = \frac{1}{S}\int_{M\in S} \frac{(\mathbf{PM}\times\mathbf{U}_M)\cdot\mathbf{z}}{\|\,\mathbf{PM}\,\|\cdot\|\,\mathbf{U}_M\,\|}\,\mathrm{d}S = \frac{1}{S}\int_S \sin\theta_M\,\mathrm{d}S \qquad (1)$$

where $\mathbf{U}_M$ is the local velocity at the point M, $\mathbf{z}$ is the unit vector normal to the measurement plane, and θ_M is the angle between the two vectors $\mathbf{PM}$ and $\mathbf{U}_M$. This criterion has values between -1 and 1, and it can be shown that the values of $|\Gamma_1| > 2/\pi$ correspond to the presence of a vortex, with the sign of Γ_1 related to the sense of rotation. In the case of PIV measurements, the vector field is discrete. We then use a rectangular interrogation area S, containing N vectors, and we approximate the previous relation by

$$\Gamma_1 = \frac{1}{S}\int_S \sin\theta_M\,\mathrm{d}S = \frac{1}{N}\sum_N \sin\theta_M \qquad (2)$$

Based on this definition, the criterion has been used for the different instantaneous fields where a convection velocity of 200 ms^{-1} has been subtracted and with an interrogation area of 4 mm^2. Typical maps of Γ_1 for the instantaneous field are reported Fig. 10 for the 8 deg case.

We also estimate the spatial average of the Γ_1 detector for the 10^4 fields recorded (see Fig. 11). This defines the region where the vortices are statistically present. Equivalent results in the 9.5 deg case are presented Fig. 12.

As expected, the location of the maximum of probability to have an eddy correspond very well with the region of high energy which develops in the interaction and in the relaxation zone (see Figs. 5 and 6). In both cases, the development of the mixing layer zone is well highlighted by the vortex detector: the initial mixing layer which develops in the first half of the recirculating region, then the creation

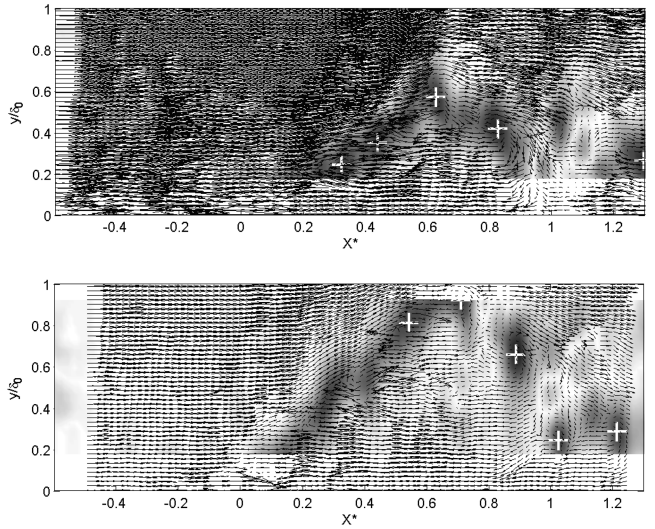

Fig. 10 Vector fields and Γ_1 vortex detector superimposed, $\theta = 8$ deg (white crosses: detected vortices).

of large vortices in the second half. It has to be noted that results for 9.5 deg are not as clear as for 8 deg; if the global behavior is very similar, the Γ_1 detector seems to fail to clearly identify the different vortical structures in this strong interaction.

These results confirm the development of large vortices in this region and illustrate some important similarities between the recirculating bubble in subsonic and supersonic cases. At low speed, it is well known that the separated flow experiences large unsteadiness at very low frequency (also called "flapping" motions). It can be observed in Figs. 10 and 12 that such a behavior is also present in our case: the instantaneous fields of Γ_1 present differences

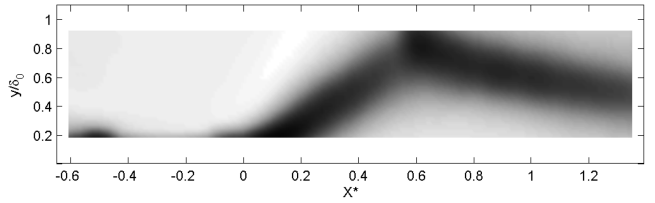

Fig. 11 Map of equiprobability of structures presence, $\theta = 8$ deg.

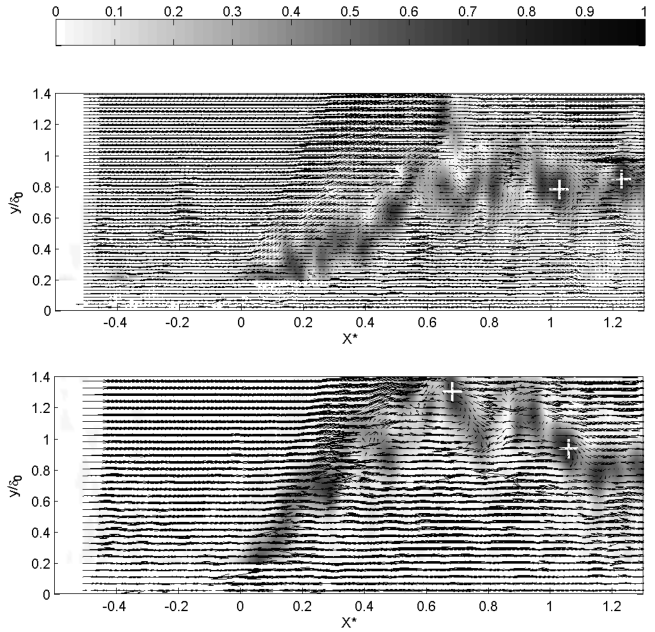

Fig. 12 Vector field and Γ_1 vortex detector superimposed, $\theta = 9.5$ deg (white crosses: detected vortices).

of large vertical motions, at least on the order of one-half boundary-layer thickness.

As these PIV measurements are not resolved in time, it is not possible to define a time scale for these oscillations of the mixing layer zone. For this reason, we have attempted to correlate these movements to the reflected shock motions. The instantaneous reflected shock positions have been estimated at a point near the edge of the layer. In this region, the upstream and downstream fluctuations of the normal velocity v are negligible with respect to the step of velocity across the shock. Therefore, it is possible to localize the front of the shock at the beginning of the rapid increase of the normal velocity. Simultaneously, the thickness of the recirculating zone has been characterized with the elevation of the region of convected vortices. It has been estimated from the map of the Γ_1 detector and chosen as the highest position of the vortices which are developing in the initial mixing layer, just before they are shed into the downstream flow.

We determined from our PIV measurements the correlation between the instantaneous position of the shock and the thickness of the recirculating zone for a set of 200 realizations. Their repartition is shown in Fig. 13, where both quantities have been centered and normalized to their rms value. A significant link emerges: the associated correlation coefficient is about -0.5. When the recirculating bubble is dilating, the reflected shock moves upstream, and when the bubble is contracting, the shock moves downstream.

Moreover, statistical links between the reflected shock and the recirculating bubble have already been observed with unsteady wall pressure measurements. For example, we report in Fig. 14 the coherence functions measured with several Kulite sensors in the 9.5 deg case. The reference probe is localized at the median position of the foot of the reflected shock, when the other probes are placed in the second half of the separating bubble. A strong coherence exists between both regions (Coh ≈ 0.85) in the range of the shock oscillations frequencies (around 150 Hz), which is consistent with the links observed by PIV.

Other authors [10,23] have already proposed a very similar scheme in compression ramp flows from unsteady wall pressure measurements.

IV. Conclusions

The results presented in this paper give an overview of an incident shock-wave-induced separation for different shock intensities. The velocity fields are obtained by PIV. The accuracy of the measurements is validated in the upstream boundary layer by comparison with LDA measurements. The mean and the instantaneous fields give a global picture of the spatial organization of the interaction: the reflected shock is unsteady and large

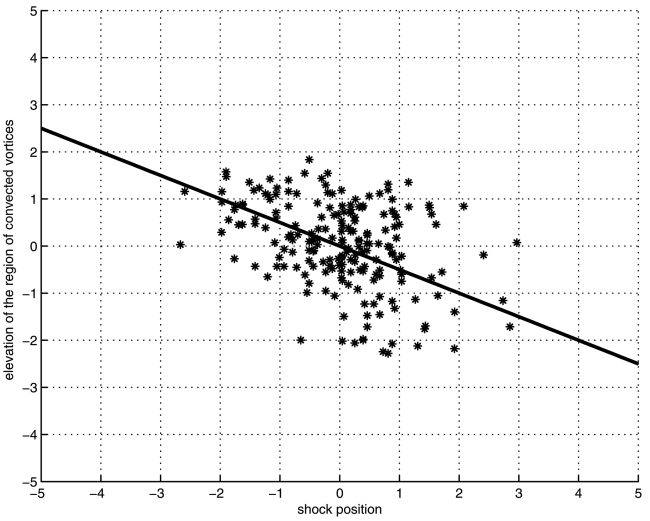

Fig. 13 Statistical link between the reflected shock motion and the flapping of the mixing layer in the recirculation zone.

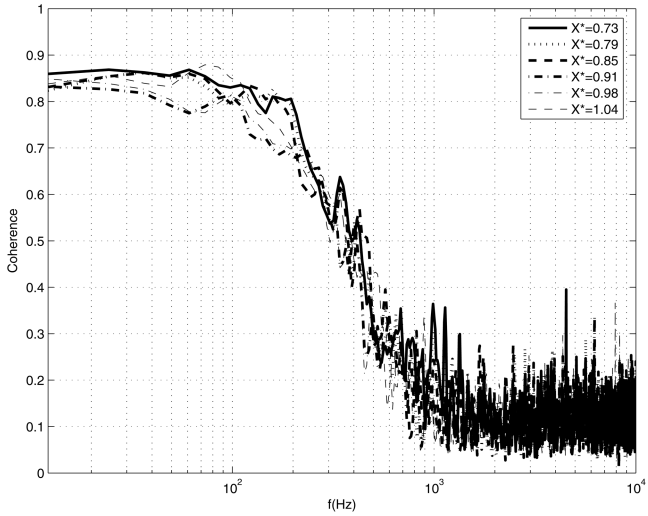

Fig. 14 Coherence function between wall pressure signals recorded in the vicinity of the reflected shock and near the reattachment region, $\theta = 9, 5$ deg, from [6,11].

convective scales develop in the mixing layer formed from the separation line. The wavelength of these structures is about $0.2–0.4L$. It seems that larger shock intensities produce more complicated velocity fields, for which a clear identification of convected eddies becomes more difficult. A new result is the evidence of large amplitude vertical movements of this region, identified as flapping, which have a significant correlation with the reflected shock movements. Such a scheme was already proposed in other works in the case of compression ramp flows. This confirms that the low-frequency unsteady behavior of shock-induced-separated flows (compression ramps, incident shock waves, blunt fins, etc.) present some important common features. The physical basis of this large unsteadiness of the recirculating bubble is still an important open question for shock-induced-separated flows, as well as for subsonic detached flows. It is now necessary to improve the different eduction schemes used (vortex detector and instantaneous shock front) to automate their detection for processing the entire data set available (10^4 fields). This will help clarify the coupling between the shock oscillations with the downstream recirculating zone, and possibly with the upstream boundary layer.

Acknowledgments

Part of this work was carried out with the support of the Research Pole ONERA/Centre National d'Etudes Spatiales *Aérodynamique des Tuyères et Arrière-Corps* and of the European Strategic Research European Program Unsteady Effects in Shock Wave Induced Separation. Their support is gratefully acknowledged. The author, A. Sidorenko, was supported by the European Program International Association for the promotion of cooperation with scientists from the New Independent States of the former Soviet Union for his stay at Institut Universitaire des Systèmes Thermiques Industriels. Comments of J. P. Dussauge are also gratefully acknowledged.

References

[1] Delery, J., and Marvin, J. G., "Shock Wave–Boundary Layer Interactions," NATO, AGARDograph No. 280, 1986.

[2] Smits, A. J., and Dussauge, J. P., *Turbulent Shear Layers in Supersonic Flow*, 2nd ed., AIP Press, Springer, New York, 1996.

[3] Dolling, D. S., "Fifty Years of Shock-Wave/Boundary-Layer Interaction Research: What Next," *AIAA Journal*, Vol. 39, No. 8, 2001, pp. 1517–1531.

[4] Lee, B. H. K., "Self Sustained Oscillations on Airfoils at Transonic Speeds," *Progress in Aerospace Sciences*, Vol. 37, Feb. 2001, pp. 147–196.
doi:10.1016/S0376-0421(01)00003-3

[5] Dupont, P., Haddad, C., Ardissone, J. P., and Debiève, J. F., "Space and Time Organization of a Shock Wave/Turbulent Boundary Layer Interaction," *Aerospace Science and Technology*, Vol. 9, No. 7, 2005, pp. 561–572.
doi:10.1016/j.ast.2004.12.009

[6] Haddad, C., "Instationnarités, Mouvements donde de Choc et Tourbillons à Grande Échelles dans une Interaction onde de Choc/Couche Limite avec Décollement," Ph.D. Thesis, Univ. de Provence Aix-Marseille I, Marseille, France, 2005.

[7] Ganapathisubramani, B., Clemens, N. T., and Dolling, D. S., "Planar Imaging Measurements to Study the Effect of Spanwise Structure of Upstream Turbulent Boundary Layer on Shock Induced Separation," *44th AIAA Aerospace Sciences Meeting and Exhibit*, AIAA Paper 2006-324, 2006.

[8] Beresh, S. J., Clemens, N. T., and Dolling, D. S., "Relationship Between Upstream Turbulent Boundary Layer Velocity Fluctuations and Separation Shock Unsteadiness," *AIAA Journal*, Vol. 40, No. 12, 2002, pp. 2412–2422.

[9] Andreopoulos, J., and Muck K. C, "Some New Aspects of the Shock Wave–Boundary Layer Interaction in Compression Ramp Flows," *Journal of Fluid Mechanics*, Vol. 180, July 1987, pp. 405–428.
doi:10.1017/S0022112087001873

[10] Thomas, F. O., Putman, C. M., and Chu, H. C., "On the Mechanism of Unsteady Shock Oscillation in Shock Wave/Turbulent Boundary Layer Interaction," *Experiments in Fluids*, Vol. 18, Dec. 1994, pp. 69–81.
doi:10.1007/BF00209362

[11] Dupont, P., Haddad, C., and Debiève, J. F., "Space and Time Organization in a Shock Induced Boundary Layer," *Journal of Fluid Mechanics*, Vol. 559, July 2006, pp. 255–277.
doi:10.1017/S0022112006000267

[12] Dussauge, J. P., Dupont, P., and Debiève, J. F., "Unsteadiness in Shock Wave Boundary Layer Interactions with Separation," *Aerospace Science and Technology*, Vol. 10, March 2006, pp. 85–91.
doi:10.1016/j.ast.2005.09.006

[13] Robinet, J. C., "Bifurcations in Shock Wave/Laminar Boundary Layer Interaction: Global Instability Approach," *Journal of Fluid Mechanics*, Vol. 579, May 2007, pp. 85–112.
doi:10.1017/S0022112007005095

[14] Garnier, E., and Sagaut, P., "Large Eddy Simulation of Shock/Boundary Layer Interaction," *AIAA Journal*, Vol. 40, No. 10, 2002, pp. 1935–1944.

[15] Pirozzoli, S., and Grasso, F., "Direct Numerical Simulation of Impinging Shock Wave/Turbulent Boundary Layer Interaction at $M = 2.25$," *Physics of Fluids*, Vol. 18, No. 6, June 2006, p. 065113.
doi:10.1063/1.2216989

[16] Wu, M., and Martin, P., "Direct Numerical Simulation of Supersonic Turbulent Boundary Layer over a Compression Ramp," *AIAA Journal*, Vol. 45, No. 4, 2007, pp. 879–889.
doi:10.2514/1.27021

[17] Deleuze, J., and Elena, M., "Some Turbulence Characteristics Downstream a Shock Wave-Boundary Layer Interaction," *Proceedings of the 6th European Turbulent Conference*, Kluwer Academic, Norwell, MA, July 1996, pp. 433–436.

[18] Elena, M., Tedeschi, G., and Gouin, H., "Motion of Tracer Particles in Supersonic Flows," *Experiments in Fluids*, Vol. 26, No. 4, 1999, pp. 288–296.
doi:10.1007/s003480050291

[19] Laurent, H., "Turbulence dune Interaction onde de Choc-Couche Limite sur Paroi Plane Adiabatique ou Chauffée," 3ème cycle Thesis, Univ. de Aix-Marseille II, Marseille, France, 1996.

[20] Benkemoun, L., and Salaun, M., "Développement dune Couche Limite Turbulente Supersonique sur une Paroi Chauffée. Propriétés du Champ Tubulent et Exploitation Théorique," ONERA Rept. n74/7078, 1988.

[21] Kiya, M., and Sasaki, K., "Structure of a Turbulent Separation Bubble," *Journal of Fluid Mechanics*, Vol. 137, Dec. 1983, pp. 83–113.
doi:10.1017/S002211208300230X

[22] Graftieaux, L., Michard, M., and Grosjean, N., "Combining PIV, POD and Vortex Identification Algorithms for the Study of Unsteady Turbulent Swirling Flows," *Measurement Science and Technology*, Vol. 12, No. 9, 2001, pp. 1422–1429.
doi:10.1088/0957-0233/12/9/307

[23] Gramann, R. A., and Dolling, D. S., "Dynamics of Separation and Reattachment in a Mach 5 Unswept Compression Ramp Flow," *AIAA 28th Aerospace Sciences Meeting*, AIAA Paper 90-0380, 1990.